Journal of *Marine Science and Engineering*

MDPI

Article

Influence of the Spatial Pressure Distribution of Breaking Wave Loading on the Dynamic Response of Wolf Rock Lighthouse

Darshana T. Dassanayake [1,2,*], Alessandro Antonini [3], Athanasios Pappas [4], Alison Raby [2], James Mark William Brownjohn [5] and Dina D'Ayala [4]

1 Department of Civil and Environmental Technology, Faculty of Technology, University of Sri Jayewardenepura, Pitipana 10206, Sri Lanka
2 School of Engineering, Computing and Mathematics, University of Plymouth, Drake Circus, Plymouth PL4 8AA, UK; alison.raby@plymouth.ac.uk
3 Faculty of Civil Engineering and Geosciences, Delft University of Technology, Stevinweg 1, 2628 CN Delft, The Netherlands; a.antonini@tudelft.nl
4 Department of Civil, Environmental and Geomatic Engineering, Faculty of Engineering Science, University College London, Gower Street, London WC1E 6BT, UK; a.pappas@ucl.ac.uk (A.P.); d.dayala@ucl.ac.uk (D.D.)
5 College of Engineering, Mathematics and Physical Sciences, University of Exeter, Exeter EX4 4QF, UK; J.Brownjohn@exeter.ac.uk
* Correspondence: darshana.dassanayake@sjp.ac.lk

Abstract: The survivability analysis of offshore rock lighthouses requires several assumptions of the pressure distribution due to the breaking wave loading (Raby et al. (2019), Antonini et al. (2019). Due to the peculiar bathymetries and topographies of rock pinnacles, there is no dedicated formula to properly quantify the loads induced by the breaking waves on offshore rock lighthouses. Wienke's formula (Wienke and Oumeraci (2005) was used in this study to estimate the loads, even though it was not derived for breaking waves on offshore rock lighthouses, but rather for the breaking wave loading on offshore monopiles. However, a thorough sensitivity analysis of the effects of the assumed pressure distribution has never been performed. In this paper, by means of the Wolf Rock lighthouse distinct element model, we quantified the influence of the pressure distributions on the dynamic response of the lighthouse structure. Different pressure distributions were tested, while keeping the initial wave impact area and pressure integrated force unchanged, in order to quantify the effect of different pressure distribution patterns. The pressure distributions considered in this paper showed subtle differences in the overall dynamic structure responses; however, pressure distribution #3, based on published experimental data such as Tanimoto et al. (1986) and Zhou et al. (1991) gave the largest displacements. This scenario has a triangular pressure distribution with a peak at the centroid of the impact area, which then linearly decreases to zero at the top and bottom boundaries of the impact area. The azimuthal horizontal distribution was adopted from Wienke and Oumeraci's work (2005). The main findings of this study will be of interest not only for the assessment of rock lighthouses but also for all the cylindrical structures built on rock pinnacles or rocky coastlines (with steep foreshore slopes) and exposed to harsh breaking wave loading.

Keywords: breaking wave loading; impact pressure distributions; offshore vertical cylinders; lighthouses; STORMLAMP project

Citation: Dassanayake, D.T.; Antonini, A.; Pappas, A.; Raby, A.; Brownjohn, J.M.W.; D'Ayala, D. Influence of the Spatial Pressure Distribution of Breaking Wave Loading on the Dynamic Response of Wolf Rock Lighthouse. *J. Mar. Sci. Eng.* **2021**, *9*, 55. https://doi.org/10.3390/jmse9010055

Received: 30 November 2020
Accepted: 26 December 2020
Published: 6 January 2021

1. Introduction

Offshore rock lighthouses constructed during the Victorian era by the British engineers are constructed from masonry interlocking blocks. These towers mark submerged or low-lying offshore rock pinnacles, otherwise difficult to observe from a vessel bridge. In addition to being indispensable permanent aids for navigation, these structures are of incalculable cultural significance. The majority of these towers are subjected to direct wave impacts during severe storms. The offshore rocks typically consist of steep foreshores and pinnacles

that are barely sufficient in area for the tower foundations. This shoal geometry forces the incoming waves to break either in close proximity to the base of the lighthouse or directly onto the tower, causing unwanted dynamic structural responses which threaten the stability of these structures. Historical anecdotes of former lighthouse keepers provide vital evidence of substantial past impact events. On some occasions, the accelerations due to structure responses could reach values equivalent to modest earthquakes (Raby et al. (2019) [1]). The most sensible method to assess the dynamics of multi-block structure responses due to extreme weather events is by means of a validated 3D distinct element model (DEM) (Pappas et al. (2018) [2]). The external force exerted on the surface of the structure is one of the crucial input parameters that governs the accuracy of the model predictions. However, there are no dedicated formulae to accurately quantify the loads induced by breaking waves for such peculiar configurations.

Overall breaking wave forces acting on offshore monopiles can be estimated using Wienke's formula (Wienke and Oumeraci (2005) [3]); however, this formula is sensitive to wave-induced pressure distribution on the surface of the structure. The wave-induced pressure distribution of an offshore monopile and an offshore lighthouse have significant differences, as wave kinematics for a breaking wave on a shoal are much more complex compared to offshore breaking waves in deeper water. Therefore, dynamic responses of lighthouses might be vastly different to those of offshore monopiles. Detailed numerical modelling of rock lighthouses are rare; therefore, the most probable synthetic pressure distributions were tested using the validated Wolf Rock DEM model (Raby et al. (2019) [1]). The main findings are of interest not only for the assessment of the survivability of rock lighthouses but also for all the cylindrical structures built on rock pinnacles or rocky coastlines (with steep foreshore slopes) and exposed to the harsh breaking wave loadings.

The Wolf Rock lighthouse is located approximately 13.5 km south-southwest of the most south-westerly tip of mainland UK. It stands 35.33 m from the foundation to the gallery level (70 rock masonry courses), the lowest 11.98 m (20 courses) being solid except for a water tank. The lighthouse consists of characteristic concave elliptic frustum curve with a maximum diameter of 12.2 m at its base (1st course), which gradually decreases to 5.2 m (67th course). The lowest 20 courses are of a stepped design, with this feature considered as an effective effort to reduce wave runup (Raby et al. (2019), Boyle (1998) [1,4]). After the 67th course, the tower widens again to reach 6.4 m diameter at the 70th course with a recurved profile (radius = 1.15 m) intended to divert the up-rushing wave from the gallery. James Walker initiated the designing of Wolf Rock lighthouse in 1860 based on his prior design and construction experiences on similar rock towers such as Bishop Rock and the Smalls lighthouses (Nicholson (2015) [5]). The design (Figure 1a) was completed by William Douglass in 1862 (Douglas (1870, 1871) [6,7]). In 1870, the lighthouse construction was completed after a slow and long construction process due to the severe constraints of working on such a small and low-lying rock exposed to Atlantic gales. This engineering masterpiece has withstood the forces of the ocean since then without requiring any major repairs, but with rigorous inspections and maintenance routines conducted by Trinity House. The UK and Irish General Lighthouse Authorities (GLAs), namely The Corporation of Trinity House, the Northern Lighthouse Board and the Irish Lights (responsible for England, Wales, the Channel Islands and Gibraltar; Scotland; and Northern Ireland and the Republic of Ireland, respectively), need to systematically study the conditions of these heritage structures, primarily focusing on the remaining operational life in light of climate change, with the increase in sea level and the possibility of increased storminess (frequency and magnitude). Therefore, the STORMLAMP project, funded by the UK Engineering and Physical Sciences Research Council (EPSRC), selected Wolf Rock lighthouse (Figure 1b) as one of the seven lighthouses investigated under the project (Raby et al. (2019) [1], Antonini et al. (2019) [8]). This study investigated the differences in the dynamic structure responses of offshore rock lighthouses due to different pressure distributions. The impact area was kept constant in this study, and different impact pressure distributions were tested

using a validated DEM. This study considers the theoretical total impact force based upon Wienke's formula (Wienke and Oumeraci (2005) [3]).

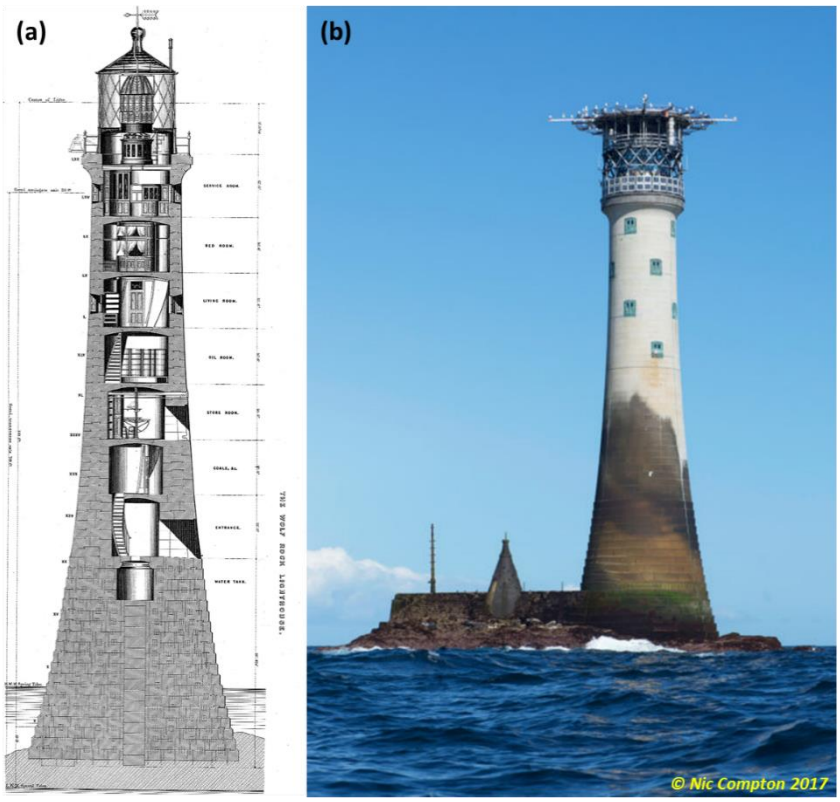

Figure 1. Wolf Rock lighthouse: (**a**) drawing by James Douglas (1870) [6] and (**b**) Wolf Rock lighthouse in 2017 (reproduced by kind permission of Nic Compton).

From a structural engineering point of view, it is essential to know the implications of different pressure distributions on the dynamic structural responses and ultimately on the overall structural stability of lighthouses. Trinh et al. (2016) and Banfi (2017) [9,10] studied the dynamic response of the Eddystone lighthouse numerically and experimentally. These studies were further combined with analysis of field data (i.e., wave buoy data, geophone data and video camera footage) to enhance the accuracy of the model results. The theory of Wienke and Oumeraci (2005) [3] was implemented in their study with the triangular vertical distribution, as suggested by Tanimoto et al. (1986) [11], to simulate impulsive breaking wave loads. Their finite element model (FEM) correctly reproduced similar displacement time series and amplitude spectra to those extracted from the geophone data. Trinh et al. (2016) [9] performed a parametric study using their validated 3D FEM and concluded that the point of application of the wave load is highly important in the tower's structural response. However, the 3D FEM of Trinh et al. (2016) [9] was a simplified representation of the lighthouse structure and did not accurately represent the details of the gallery and the helideck. The aforementioned studies identified several key parameters to describe an impact event due to wave loading and also showed the path forward for future studies.

The current study aims to identify how the assumed pressure distributions affect the dynamic response of the lighthouse using the state-of-the-art 3D "distinct element method" (DEM) taking into account all the fine details of the gallery, the helideck and the vertical and horizontal keys and dovetail connections between the granite blocks. The paper sections are structured as follows: Section 2 describes the available methods to estimate the impulsive loads and the pressure distributions in the literature; Section 3 presents the adopted pressure distributions and the analysis performed to identify the total impulsive wave loading; Section 4 provides details of the Wolf Rock lighthouse DEM;

Section 5 presents the main results coming from the structure analysis, highlighting the influence of the tested pressure distributions; and Section 6 summarises the findings of this study, with concluding remarks, and shows the path forward.

2. Impulsive Wave Loading Description

The hydrodynamics of breaking wave interactions with an offshore monopile is a complex 3D phenomenon (Veić and Sulisz (2018) [12]). An offshore rock lighthouse on a partially emerged rocky shoal adds more complexity to the phenomenon due to (i) the irregular bathymetry and topography of the rock shoal, which governs wave refraction, shoaling and breaking; and (ii) the unique geometry of the Victorian rock lighthouses, which are typically tapered cylindrical towers with steps in the first 10–15 m height to form a curved concave profile (typically described as the shape of an English Oak tree (Trinity House (2016) [13]). Different combinations of shoal geometries, lighthouse geometries and wave parameters (water level, wave height, wave period) might exert different impact pressure distributions on the lighthouse surface, consequently resulting in different dynamic responses. In this work, in order to provide a pragmatic method to quantify the impulsive wave loading on the offshore lighthouses, we simplify the depiction of the loading phenomena by adopting well-known empirical models for the description of the local wave conditions, i.e., Goda (2010) [14] and Battjes and Groenendijk (2000) [15], while at the same time Wienke's method for the description of the impulsive load takes into account the spatial variability of the structure's perimeter. A detailed investigation of the impact pressure distributions (spatial and temporal) can only be achieved through a thorough Computational Fluid Dynamics (CFD) model of the real lighthouse and shoal geometry. A CFD study should essentially be supported either by experimental data or field measurements for its calibration and validation. A large-scale physical model might also be able to provide a satisfactory data set if a good spatial resolution in pressure measurements can be achieved. Prior to such a comprehensive investigation on the impact pressure distribution, it is essential to evaluate the sensitivity of rock lighthouses to different pressure distributions in order to validate or to challenge the current common assumption of uniform pressure distribution across the (theoretical) impact area. The dynamic structural responses of rock lighthouses provide a quantitative measure of the influence of impact pressure distributions. Morison et al. (1950) [16,17] developed an equation to estimate the forces exerted on a circular monopile exposed to deep water waves (Equation (1)). The original Morison formula was developed for non-breaking waves, where the total force is the sum of drag force (F_D) and inertia force (F_M) (Equation (1)) acting on a vertical cylinder.

$$F = F_D + F_M = \frac{1}{2}\int_{-d}^{\eta} \rho_w C_D D u|u| dz + \int_{-d}^{\eta} \rho_w C_M \frac{\pi D^2}{4} \frac{\partial u}{\partial t} dz, \quad (1)$$

where, F = total force, F_D = drag force, F_M =inertia force, ρ_w = water density, C_D = drag coefficient, C_M = inertia coefficient, η = water surface elevation, d = depth, D = diameter of the cylinder, u = velocity and t = time. Morison's equation is generally valid for slender cylinders where the ratio of wavelength to monopile diameter is larger than 5 (which is the case for offshore rock lighthouses). The inertia force is due to the acceleration of wave–structure interaction-induced flow, while the drag component is associated with the flow velocity. The coefficients C_D and C_M can be empirically determined by through laboratory experiments. The drag and the inertia coefficients are typically in the ranges $0.6 < C_D < 1.2$ and $1.6 < C_M < 2.0$, respectively (DNV (2014) [18]).

However, the total force exerted on an offshore monopile can be much higher than that predicted by the Morison's equation. This higher force occurs when a wave breaks onto the cylinder or when the waves are strongly non-linear, as highlighted by Corvaro et al. (2019) [19], initially exerting a slamming force for a fraction of second, followed by a less impulsive part of longer duration. Therefore, breaking wave forces can be divided into two components: an impact force (or slamming force) component and a quasi-static component.

The quasi-static components can be fully described using Morison's equation ($F_D + F_M$), but not the impact force (F_I), as highlighted by several authors such as Goda et al. (1966), Chaplin et al. (1992), Wienke (2001) and Ghadirian and Bredmose (2019) [20–23]. Morison's force ($F_D + F_M$) model was extended with an additional impact force component (F_I) to account for breaking wave forces, calculated using Equation (2).

$$F = F_D + F_M + F_I \quad (2)$$

where F = total force, F_D = drag force, F_M = inertia force and F_I = impact force. The magnitude of the maximum impact force is larger than what can be estimated considering the momentum conservation during the impact mainly due to the deformation of the water surface and the reduction in impact duration. The impact force is often characterised by a sudden peak, followed by a temporal decay. Goda et al. (1966) [20] proposed a model for the impact force by considering the breaking wave as a vertical wall of water hitting the cylinder with a speed equal to the wave celerity (C). Only the upper part of the wave crest is (assumed to be) responsible for the impact force; this is defined by the curling factor, λ, as shown in Figure 2. The height of the impact area ($\lambda \cdot \eta_{max}$) is related to the maximum water surface elevation (η_{max}) through the curling factor (λ). The impact force is assumed to be equally distributed along the impact height.

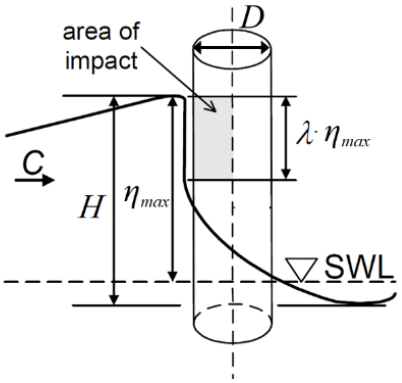

Figure 2. Definition sketch for an offshore breaking wave impact (Goda et al. (1966) [20]).

Equation (3) estimates the maximum impulsive force acting on a cylinder according to Goda's method. The curling factor depends on the breaker type as it represents the portion of the wave crest (η_{max}) over which the impact force acts on the cylinder. In the case of plunging breakers, which is expected to be the most critical condition for load intensity, Goda et al. (1966) [20] estimated a value of λ = 0.4 for vertical piles. Wiegel (1982) [24] subsequently recommended a value of λ = 0.5 for similar breaker types, which will lead to an over-estimation of the wave loads if Goda's method correctly calculates those values. The peak impact force occurs when the breaker front first makes contact with the vertical cylinder, at time $t = 0$, and then the impact force linearly decays as the breaker front propagates further.

$$F_I = \rho_w \frac{D}{2} C^2 \left\{ \pi \left(1 - \frac{2C}{D} t \right) \right\} \lambda \eta_{max} \quad (3)$$

where ρ_w = density of the water; D = diameter of the pile; C = wave celerity; λ = curling factor; η_{max} = maximum water surface elevation; and t = time.

Since Goda et al. (1966) [20], research work of Watanabe and Horikawa (1974) [25], Sawaragi and Nochino (1984) [26], Tanimoto et al. (1986) [11]), Apelt and Piorewiez (1991) [27], etc., enhanced the understanding of wave–cylinder interactions. A time-dependent empirical coefficient called the "slamming coefficient (Cs)" was introduced to

describe the impact force (Equation (4)). Since then, the research focus was to define the slamming coefficient.

$$F_I = \rho_w \frac{D}{2} C_b^2 C_s \lambda \eta_{max} \tag{4}$$

where C_b = wave celerity at breaker point, and C_s = ("time-dependent") slamming coefficient.

One of the most comprehensive descriptions of breaking wave impacts on vertical cylinders was developed by Wienke (2001) [22] and Wienke and Oumeraci (2005) [3]. Wienke (2001) [22] investigated the curling factor (λ) values proposed by Goda (1966) [20] and Wiegel (1982) [24] for plunging breakers through a series of large scale experiments. The mean curling factor for the maximum loading case due to plunging breakers was found to be λ = 0.46. Moreover, a 3D force model was developed to describe the impact force (F_I) induced by a breaking wave on vertical and inclined slender cylinders. This force model (Equations (4) and (5)) can be understood by considering the definition sketch inFigure 2. According to Wienke and Oumeraci (2005) [3], the impact force is governed by the distance between the breaking location and the cylinder. The maximum impact force on the cylinder occurs when the wave breaks immediately in front of the cylinder. The velocity (V) of the water mass striking the cylinder reaches the value of the wave celerity (C) at the breaking location ($V = C_b$). The main drawback of this formula is that the breaking wave impact force is proportional to the curling factor, which has to be determined experimentally (Alagan Chella et al. (2019) [28]).

A rock lighthouse can be represented as a vertical cylinder, and then Equations (5) and (6) (Wienke and Oumeraci (2005) [3)] can be used to calculate the maximum impact force considering wave slamming load (when $V = C_b$). The terms within the parenthesis are equivalent to the time-dependent slamming coefficient (C_s).

$$\text{for } 0 \le t \le \frac{1}{16}\frac{D}{C_b}$$

$$F_{Imax} = \rho_w \frac{D}{2} {C_b}^2 \left(2\pi - 2\sqrt{\frac{2C_b}{D}} t \cdot arctanh \sqrt{1 - \frac{1}{2}\frac{C_b}{D} t} \right) \lambda \eta_{max} \tag{5}$$

$$\text{for } \frac{3}{64}\frac{D}{C_b} \le t' \le \frac{12}{64}\frac{D}{C_b} \text{ with } t' = t - \frac{1}{64}\frac{D}{C_b} :$$

$$F_{Imax} = \rho_w \frac{D}{2} {C_b}^2 \left(\pi \sqrt{\frac{1}{6}\frac{2}{\frac{C_b}{D} t'}} - \sqrt[4]{\frac{16}{3}} \frac{C_b}{D} t' \cdot arctanh \sqrt{1 - \frac{2C_b}{D} t' \sqrt{6\frac{2C_b}{D} t'}} \right) \lambda \eta_{max} \tag{6}$$

The maximum impact force can be calculated by estimating the slamming coefficient, C_s. Wienke and Oumeraci (2005) [3] compared maximum forces calculated by von Karman (1929) [29] and Wagner (1932) [30] theories. The maximum ("line") force calculated by applying Wagner's theory is twice the maximum "line force" (Wienke and Oumeraci (2005) [3]) calculated by von Karman's theory. Wienke and Oumeraci (2005) [3] describe this as $C_s = \pi$ according to von Karman and $C_s = 2\pi$ according to Wagner [30]. There are ongoing discussions of C_s values in the literature. Irschik et al. (2004) [31] performed further large-scale tests with a 1:10 slope and estimated a curling factor λ for shallow water conditions. By introducing a time-varying slamming coefficient, $C_s(t)$, the 3D model of Wienke and Oumeraci (2005) [3] for vertical cylinder can be further simplified to Equation (7).

$$F_I(t) = \rho_w \frac{D}{2} C_b^2 C_s(t) \lambda \eta_{max} \tag{7}$$

where η_{max} = maximum water surface elevation at breaking point. The curling factor for a 1:10 slope was found to be $0.4 < \lambda < 0.65$ (Irschik and Oumeraci (2004) [31]). The experimental results confirm the slamming coefficient found by Wagner (1932) [30], who considered the "pile-up" effect and estimated C_s $(t=0) = 2\pi$ at the beginning of the impact. Furthermore, based on Kyte and Tørum's, (1996) [32] work, which focused on vertical cylinders

upon submerged shoals, C_s was further calculated using the method proposed by Goda (1972) [33] and found equal to 6.8 (which is greater than 2π) with some scatter. According to Wienke and Oumeraci (2005) [3] and Irschik and Oumeraci (2004) [31], the peak impact occurs at $t = 0$, which is similar to Goda's theory. Goda's theory assumes the maximum value of the slamming coefficient to be $C_s = \pi$ (at $t = 0$), whereas Wienke's theory and Irschik and Oumeraci (2004) [31] estimate it to be $C_s = 2\pi$ (at $t = 0$). This behaviour has been clearly illustrated in Figure 17 in Wienke and Oumeraci (2005) [3].

Therefore, it can be considered that $C_s = 2\pi$ is a reasonable estimation for offshore rock lighthouses and the maximum impact force can be calculated using Equation (8). It can be summarised as the slamming coefficient (C_s) introduced in Equations (4) and (7), which reaches its peak at $t = 0$ and $C_s(t = 0) = 2\pi$ as per the experimental results. Therefore, the expression for the maximum impact force (F_{Imax}) is as follows (see Equation (8)):

$$F_{Imax} = \rho_w \frac{D}{2} C_b^2 (2\pi) \lambda \eta_{max} \quad (8)$$

This paper primarily discusses the distribution of force over the cylinder surface and its effects on the dynamic responses of the structure. When considering the entire wave impact event, which lasts for several seconds, the impact area on the cylinder surface (size and shape), the location of the peak pressure within the impact area and the pressure distribution pattern show significant spatial and temporal variations (Veić and Sulisz (2018) [12]). However, the slamming component of the total wave force occurs over a fraction of a second (e.g., according to Wienke and Oumeraci (2005) [3], it is only 0.07s). Therefore, the initial wave impact area and pressure distribution pattern were assumed to be remain unchanged over this duration, and the slamming component of the total force was estimated by integrating the pressure over the wave impact area. Several authors have attempted to describe the pressure distribution pattern during this initial impact. There are several experimental and numerical studies on vertical and azimuthal distribution of pressure along a vertical cylinder available in the literature, among which the contributions from Tanimoto (1986) [11] and Zhou et al. (1991) [34] are notable.

Tanimoto et al. (1986) [11] measured the vertical distribution of impact forces on cylinders with different inclinations using a series of force transducers installed along the cylinder. They observed a sharp peak in the impact force just below the wave crest and concluded that the distribution of the impact force is symmetrical and triangular. Furthermore, they introduced a simplified calculation method to estimate the impact force based on von Karman's (1929) [29] and Wagner's [30] theories.

Zhou et al. (1991) [34] replicated wave plunging by generating a frequency modulated wave packet. They reported a high degree of repeatability in terms of breaker point. Seven pressure sensors captured the impact pressure along a vertical line, and then the cylinder was rotated with 10° steps, and waves were repeated to achieve a good spatial resolution. Vertical pressure distribution plots (mean peak pressures) of three different cylinder diameters by Zhou et al. (1991) [34] were similar to the observations of Tanimoto et al. (1986) [11] for triangular vertical distributions (Zhou et al. (1991) [34]). The impact loads vary significantly with the relative location of the structure to the breaker point and possibly the trapped air dynamics (Zhou et al. (1991) [34]), which makes the development of a simple analytical model to describe pressure (or force) distribution quite laborious.

Both Wienke and Oumeraci (2005) [3] and Irshick and Oumeraci (2004) [31] presented models to calculate the total force assuming a rectangular distribution of pressure at the surface of the cylinder (Equations (5)–(7), respectively). The pressure distribution is calculated as a function of the immersed width. They adopted the "pile-up" effect (i.e., deformation of the water surface), when calculating the time-varying immersed width using their 2D impact model [3]. The height of the impact area depends on the shape of the breaking wave, which is described by the curling factor λ (Figure 2). Wienke and Oumeraci (2005) [3] used 30 pressure transducers at 3 different elevations in their experimental setup, as shown in Figure 3. The pressure–time history at a given location was calculated

according to the developed formulae (Equations (5) and (6)) and compared with the measured pressure values in Figure 3 to validate the method. The calculated pressure–time histories for four locations on the cylinder surface are shown in Figure 3 together with measured pressure–time histories from seven pressure transducers at the height of the wave crest. The calculated and the measured pressure–time histories were compared using the maximum pressure (p_{max}) and the corresponding time of occurrence (t_{pmax}), which showed relatively good agreement. Azimuthal horizontal pressure distributions recorded by Wienke and Oumeraci (2005) [3,22] were similar to those of Zhou et al. (1991) [34].

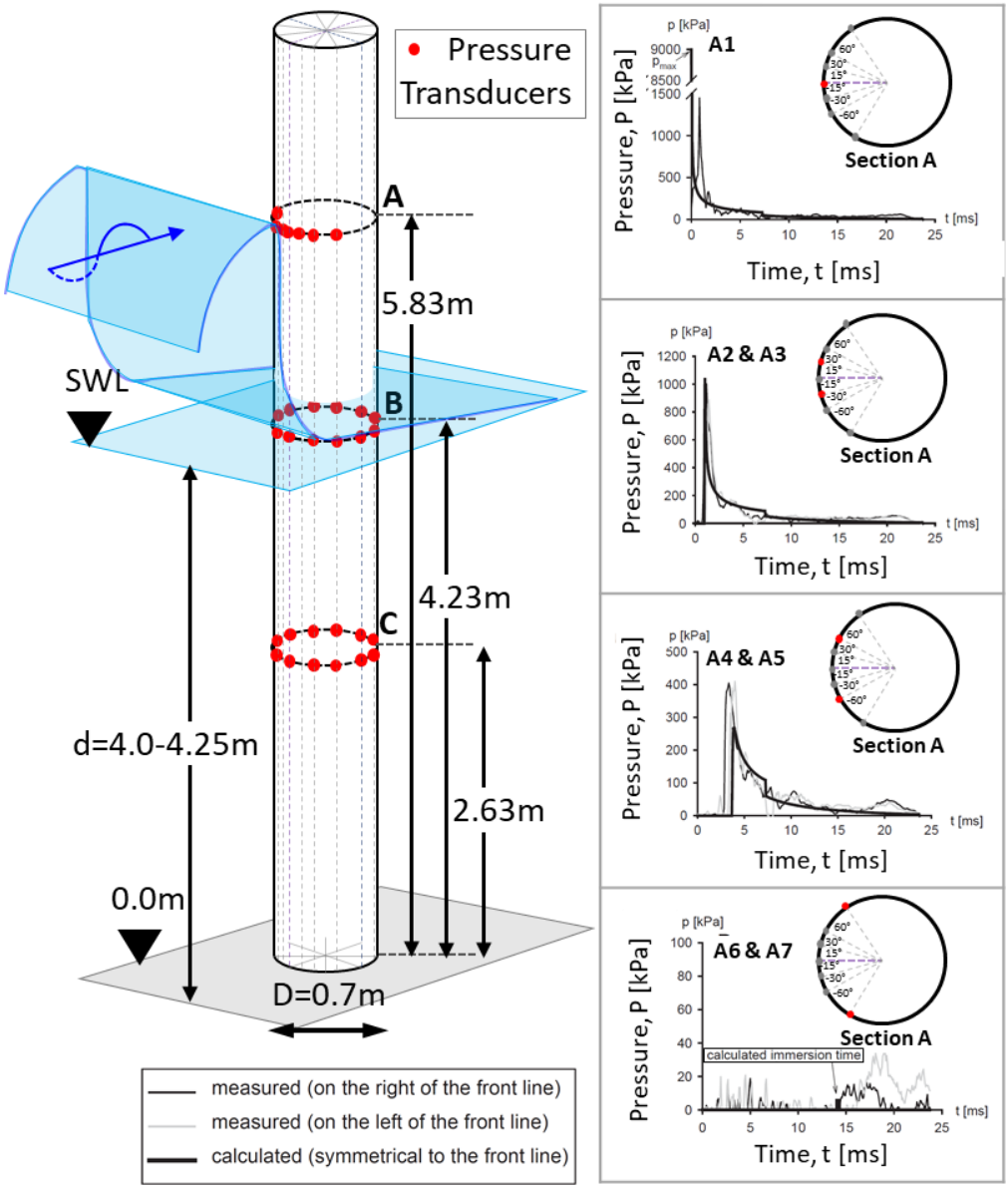

Figure 3. Azimuthal horizontal distribution of impact pressure based upon pressure measurements of Wienke and Oumeraci (2005)'s large scale experiments.

The main factors responsible for any discrepancies were identified as the entrapped air pockets between the cylinder and water surface, free surface deformation prior to the impact, entrapped air bubbles in the water, surface irregularities and sampling frequency of the pressure measurements. It was concluded that most of these effects occur only at the front line, and hence they might be neglected when the impact "line force" is considered. The time history of the impact "line force" was derived by integrating the

measured pressure values. The current study adopted azimuthal horizontal distribution from Wienke and Oumeraci (2005) [3], when developing the pressure distribution #3 (Figure 4). The distribution shape of the impact force is approximated as a triangle, which is based on the experimental results presented by Tanimoto et al. (1986) [11] and Zhou et al. (1991) [34].

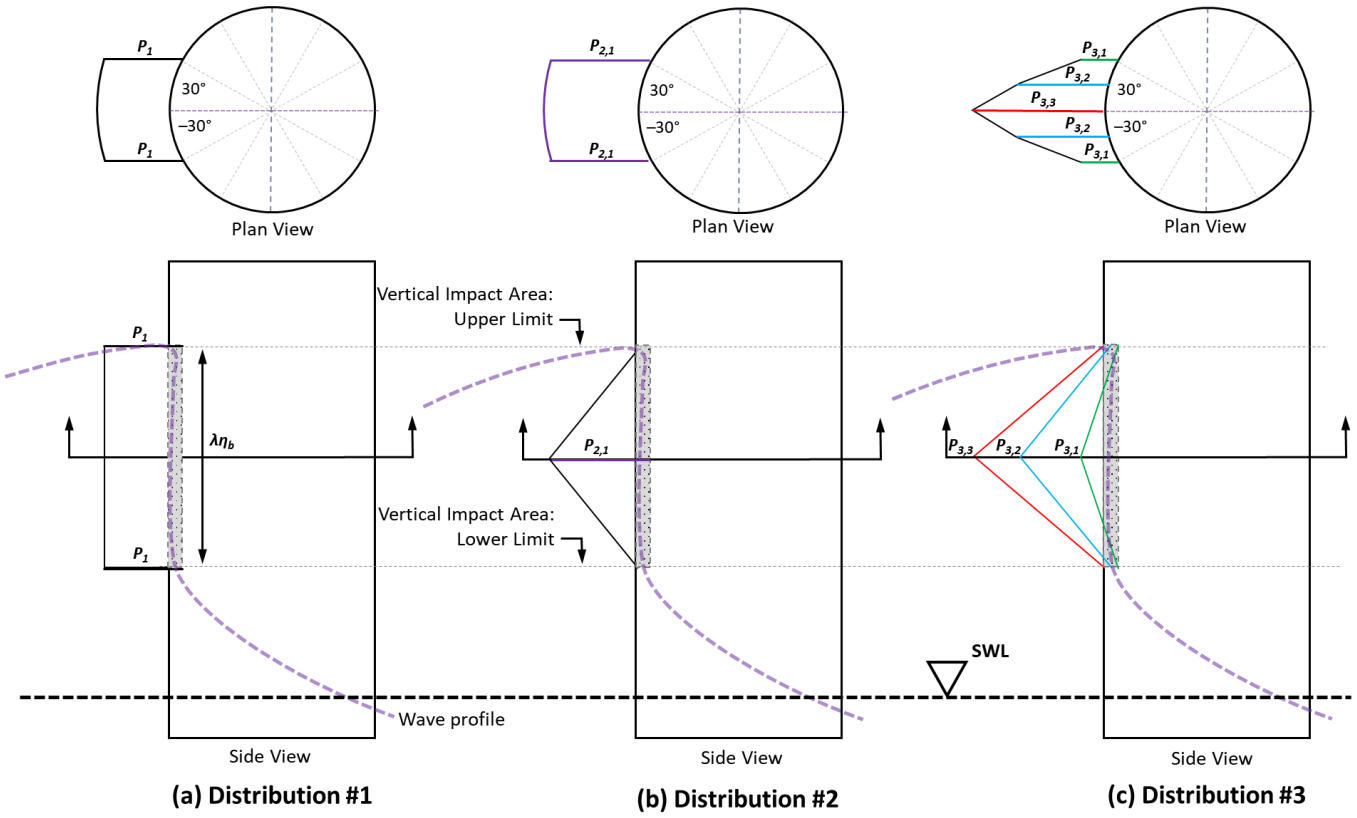

Figure 4. Pressure distribution scenarios definition sketch (adopted from Wienke and Oumeraci (2005) [3]).

Moreover, peak values of pressures measured (i.e., mean values of largest peak pressure for three tested cylinder diameters presented by Zhou et al. (1991) [34]) at ±30° azimuth angle (*when* $\theta = \pm 30°$) were less than 18% of the peak pressure values measured directly in front of the cylinder (*when* $\theta = 0°$). Therefore, impact pressure on the cylinder surface that covers an area bounded by ±30° azimuth angles (measured from the initial impact line) can represent more than 90% of the total impact force along the incident wave direction. Beyond ±30° (*when* $\theta > \pm 30°$), contributions of pressure measurements to the total impact force (force component along the incident wave direction) is less than 50% of the pressure integrated force ($\int P\delta A \cos\theta$, where $\cos\theta < 0.5$). Furthermore, the peak pressure measurements on the cylinder surface at positions $\theta = 0°$, $\theta = \pm 15°$ and $\theta = \pm 30°$ presented by Wienke and Oumeraci (2005) [3] indicate that there is also a time delay in the peak pressure measurements at different locations (Figure 3). Therefore, only the initial phase of the impact that represents ±30° impact area was considered in this study, similarly to what has been considered by Trinh et al. (2016) and Banfi (2018) [9,10] in their studies.

3. Applied Pressure Distribution Scenarios

In order to determine the total slamming load due to breaking waves, Equation (8) requires the maximum water surface elevation at breaking point (η_{max}), wave celerity at breaking point (C_b) and slamming factor (C_S). Determination of maximum water surface elevation at breaking point (η_{max}) at Wolf Rock lighthouse includes four key steps [1]. First, offshore extreme wave climate was defined based on a 24-year-long hindcast data set. This data set is a combination of a HOMERE data set (1994–2012) and NORGASUG data set

(2013–2017) made available by Ifremer (https://wwz.ifremer.fr/). Then, Goda's method (Goda (2010) [14]) provided the significant wave height for the 250-year average return period at the Wolf Rock location. Third, site-specific nearshore wave height distributions were assumed following the composite Weibull distribution (CWD) proposed by Battjes and Groenendijk (2000) [15], and $H_{0.1\%}$ was selected as the maximum individual wave height for the 250-year return period sea state. This approach might provide a slightly conservative estimation of the $H_{0.1\%}$ wave height for a submerged reef with a steep foreshore (Tuan and Cuong, (2019) [35]), but it is assumed to provide reasonable predictions considering other hydrodynamic effects associated with the rock shoal, such as wave refraction and the "focusing" effect towards the pinnacle. Moreover, the bathymetry around the Wolf Rock lighthouse does not show significant abrupt variations of the depths or multiple peaks that might induce breaking of the waves before the rock, but rather a single pinnacle with typically 1:1.5–1:3.5 slopes towards the dominant wave direction. Sea level rise is estimated to be 0.36 m at the Wolf Rock location by 2067, using the latest predictions from Palmer et al. (2018) [36]. Hansen (1990) [37] proposed a method to calculate the asymmetry between the wave crest and wave trough at the breaking point, which was applied to compute the maximum water surface elevation at breaking point (η_{max}) (with respect to the still water level).

Thus, the wave parameters that characterised the investigated impact loading event are offshore significant wave height and peak period equal to 12.85 m and 18.1 s, respectively, whereas the local significant wave height is equal to 12.25 m, characterised by $H_{0.1\%}$ equal to 23.75 m, which in turns generate a wave crest of 17.19 m. Finally, under the assumption of a curling factor equal to 0.46, the lighthouse area affected by the impulsive load extends between 9.28 m and 17.19 m.

Wave celerity at the breaker point is the next critical parameter that contributes to the total slamming load. During a severe storm event, water depths immediately surrounding the Wolf Rock are in the range of 0–10 m, even after including the additional storm surge elevation (Ganderton (2019); Trinity House (2019) [38,39]). These extremely shallow-water conditions at the Wolf Rock pinnacle are expected to result in non-periodic transient waves or wave bores. Therefore, in the absence of a proven wave theory applicable for offshore rock pinnacles, wave celerity at the impact instant was calculated based on the solitary wave theory proposed by Grimshaw (1971) [40]. Even though the solitary wave theory was adopted for the calculation of wave celerity (and eventually the total load at the impact location), the most appropriate governing wave theory for offshore rock pinnacles has yet to be identified

Figure 4 illustrates the pressure distribution scenarios considered during the current study, and the expressions for these pressure distributions scenarios are provided below as Equations (9)–(13). Pressure distribution #1 (Equation (9) and Figure 4a) assumed a uniform pressure distribution over a surface area of $\lambda\eta_b D\pi/6$ and total pressure integrated force equal to the calculated total force based on Wienke and Oumeraci (2005)'s method [3]. Pressure distribution #2 (Equation (10) and Figure 4b) kept the same pressure force and impact area but assumed a triangular distribution with a peak in the middle of the impact area. The pressure distribution at a particular elevation along the cylinder surface was kept constant at a given time, i.e., the horizontal distribution was uniform. The peak pressure was assumed to be in the middle of the impact area, which linearly decreased to zero towards the top and bottom boundaries of the impact area. Pressure distribution #3: a triangular (vertical) pressure distribution with a peak at the centroid of the impact area (Equation (11) and Figure 4c) was an attempt to incorporate the information available through the published experimental data from vertical cylinders considering the vertical and the azimuthal distributions by Tanimoto (1986) [11], Zhou et al. (1991) [34] and Wienke and Oumeraci (2005) [3]. This distribution kept the same pressure integrated force and the impact area as #1 and #2. A triangular (vertical) pressure distribution with a peak at the centroid of the impact area was considered, which linearly decreased to zero towards the top and bottom boundaries of the impact area. The azimuthal horizontal

distribution was adopted from Wienke and Oumeraci (2005) [3] under the assumption that the load is applied between $\theta = -30^\circ$ and $\theta = +30^\circ$. The coefficients ($C_{3,1}$, $C_{3,2}$ and $C_{3,3}$,) in Equations (11)–(13) were defined in order to achieve similar ratios between the peak pressure values as the measured values at positions $\theta = 0^\circ$, $\theta = \pm 15^\circ$ and $\theta = \pm 30^\circ$, which were those were presented in Wienke and Oumeraci (2005) [3], while ensuring the pressure integrated force was the same as #1 and #2.

Pressure Distribution #1: Uniform distribution over an azimuthal angle of 60°.

$$P_1 = \left(\frac{F_I}{\lambda \eta_{max} \frac{D}{2} \frac{2\pi}{6}} \right) = 0.1975 F_I \tag{9}$$

Pressure Distribution #2: Triangular distribution (vertical) with a peak in the middle of the impact area over an azimuthal angle of 60°.

$$P_{2,1} = P_{2,2} = 2 \left(\frac{F_I}{\lambda \eta_{max} \frac{D}{2} \frac{2\pi}{6}} \right) = 0.3950 F_I \tag{10}$$

Pressure Distribution #3: Triangular distribution (vertical) with a peak at the centroid of the impact area and over an azimuthal angle of 60°.

$$\text{For } \theta = 30^\circ$$
$$P_{3,1} = C_{3,1} \left(\frac{F_I}{\lambda \eta_{max} \frac{D}{2} \frac{2\pi}{6}} \right) = 0.16 F_I \text{ , } where\ C_{3,1} = 0.81 \tag{11}$$

$$\text{For } \theta = 15^\circ$$
$$P_{3,2} = C_{3,2} \left(\frac{F_I}{\lambda \eta_{max} \frac{D}{2} \frac{2\pi}{6}} \right) = 0.42 F_I, \ where\ C_{3,2} = 2.13 \tag{12}$$

$$\text{For } \theta = 0^\circ$$
$$P_{3,3} = C_{3,3} \left(\frac{F_I}{\lambda \eta_{max} \frac{D}{2} \frac{2\pi}{6}} \right) = 0.59 F_I, \ where\ C_{3,3} = 2.99 \tag{13}$$

where P_1 = average pressure over the impact area in distribution #1, $P_{2,1}$ and $P_{2,2}$ = peak pressure in the middle of the impact area in distribution #2, $P_{3,1}$ = peak pressure at the vertical planes at positions $\theta = \pm 30^\circ$ in distribution #3, $P_{3,2}$ = peak pressure at the vertical planes at positions $\theta = \pm 15^\circ$ in distribution #3, $P_{3,3}$ = peak pressure at the centroid of the impact area in distribution #3 and θ = azimuth angle in radians.

Finally, the total slamming load on the lighthouse (Figure 5a) was calculated using Equations (5) and (6). The extreme wave ($H_{0.1\%}$) derived from the 250-year return period sea state had a total impact duration of 0.070 s and maximum horizontal impact force, at $t = 0$ s, equal to 49,510 kN. The force–time history and the wave impact area are shown in Figure 5.

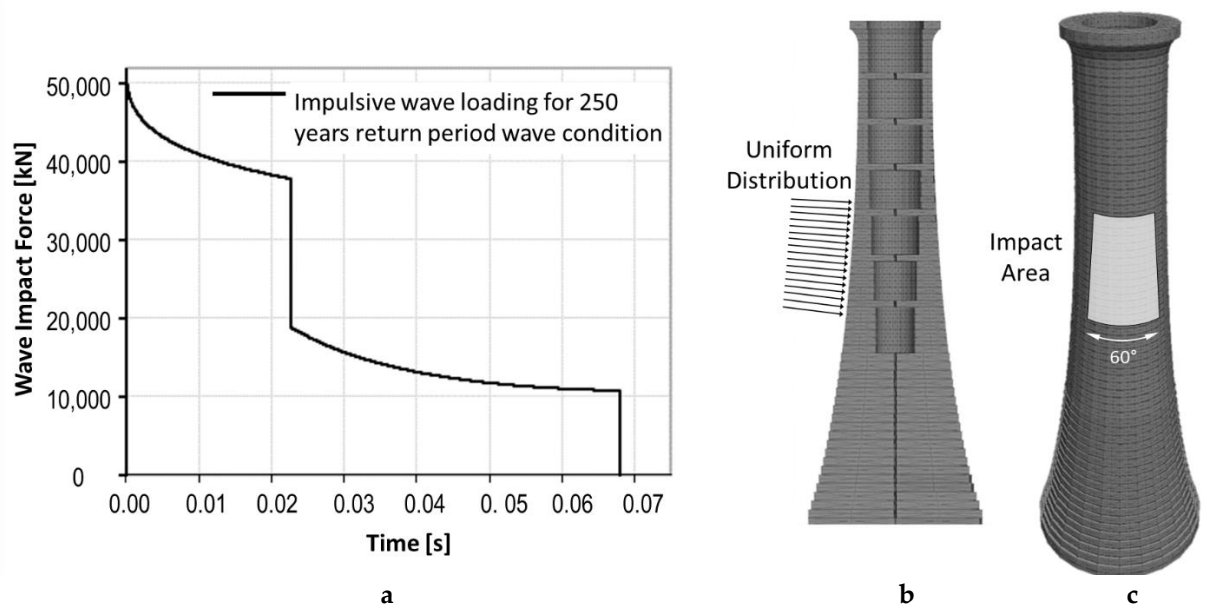

Figure 5. Wave impact force of $H_{0.1\%}$ derived from 250-year return period sea state for Wolf Rock lighthouse: (**a**) dynamic loading force–time-history; (**b**) uniform distribution of forces; (**c**) impact area.

4. Development of DEM

Victorian engineers were aware that a "lighthouse-tower might be destroyed in either of two ways, by being moved bodily by the sliding of the base upon its foundation, or by being fractured at some point in its height, and the upper portion being overthrown" (Douglass et al. (1884) [41]). The interlocking masonry system with dovetailing and vertical keys is a significant structural characteristic that contributes to the resistance of the lighthouses (Pappas et al. (2019) [42]). Dovetails connect adjacent blocks on each course, and vertical keys connect blocks of consecutive courses, with just sufficient clearance for a raised band to enter it freely in the setting. This creates a robust structural system where it is very difficult to remove a block without having removed the adjacent blocks first.

The theoretical force magnitude that is required for causing sliding or uplift, for a given position of the force, can be found based on equilibrium equations (Pappas et al. (2020) [43]). Contrary to sliding that is not reversible (but fortunately is prevented thanks to the vertical keying), uplift is reversible. However, research on the "rocking", i.e., relative rigid motion between the courses composing the structure, reveals that the phenomenon is highly nonlinear, so that the structural behaviour significantly differs compared to that of continuous structures [44–47]. The rocking theory can explain why lighthouses built with interlocked masonry can survive impacts of much higher force levels than what is expected for continuous structures.

The "distinct element method" (DEM) is an efficient method to simulate the structural response of rigid bodies that are characterised by large displacements and separation between blocks [48,49]. The method considers the structure as an assembly of blocks; the numerical solution, which produces the state position in space of each block and the forces exchanged between each couple of blocks of such assembly subjected to a system of external actions, is based on a time algorithm of small time-step cycles. The cycle consists firstly of a calculation of the block motion in terms of velocity and acceleration, which are assumed to be constant within a given time-step. As the blocks experience relative motion, new contacts between blocks are detected and the relative contact velocities and forces are updated with the use of a force–displacement law. Finally, new forces for each block centroid are calculated, and the new block motion is updated with the application of Newton's second law (Cundall, 1971) [50]. The relatively simple theory behind the DEM cycle makes the method particularly efficient for reproducing structural responses of rigid

bodies that are characterised by large displacements and separation between blocks [49–51]. Therefore, the DEM is efficient for analysing discontinuous structures such as interlocked masonry lighthouses.

A three-dimensional DEM was created with 3DEC 5.0 (three-dimensional distinct element modelling code by Itasca) [52] based on the detailed geometry of the Wolf Rock lighthouse extracted from archive drawings (Figure 6). Each course of the DEM of the lighthouse consists of 12 rigid blocks. The vertical keys are also modelled (Figure 6d), hence impeding large sliding unless significant uplift takes place. Although all blocks are rigid, the structure is deformable due to the finite stiffness of the contact interfaces. The joint normal and shear stiffnesses are equal to $7.31 \cdot 10^{10}$ Pa/m and $5.48 \cdot 10^{10}$ Pa/m, respectively. The Coulomb friction law was implemented for the joints between blocks with zero cohesion and friction angle of 30° for granite to granite contact under high compression levels (Lajtai, et al. (1989) [51]). The specific weight of the masonry blocks is taken equal to 2643 kg/m^3, based on analysis previously carried out for the Fastnet lighthouse (Pappas et al. (2017) [53]). Mass-only Rayleigh damping was applied for matching the field modal tests, which revealed a damping ratio around 0.75% at 4.67 Hz, which is the fundamental frequency for the first mode of the lighthouse (Brownjohn et al. (2018, 2019) [54,55]).

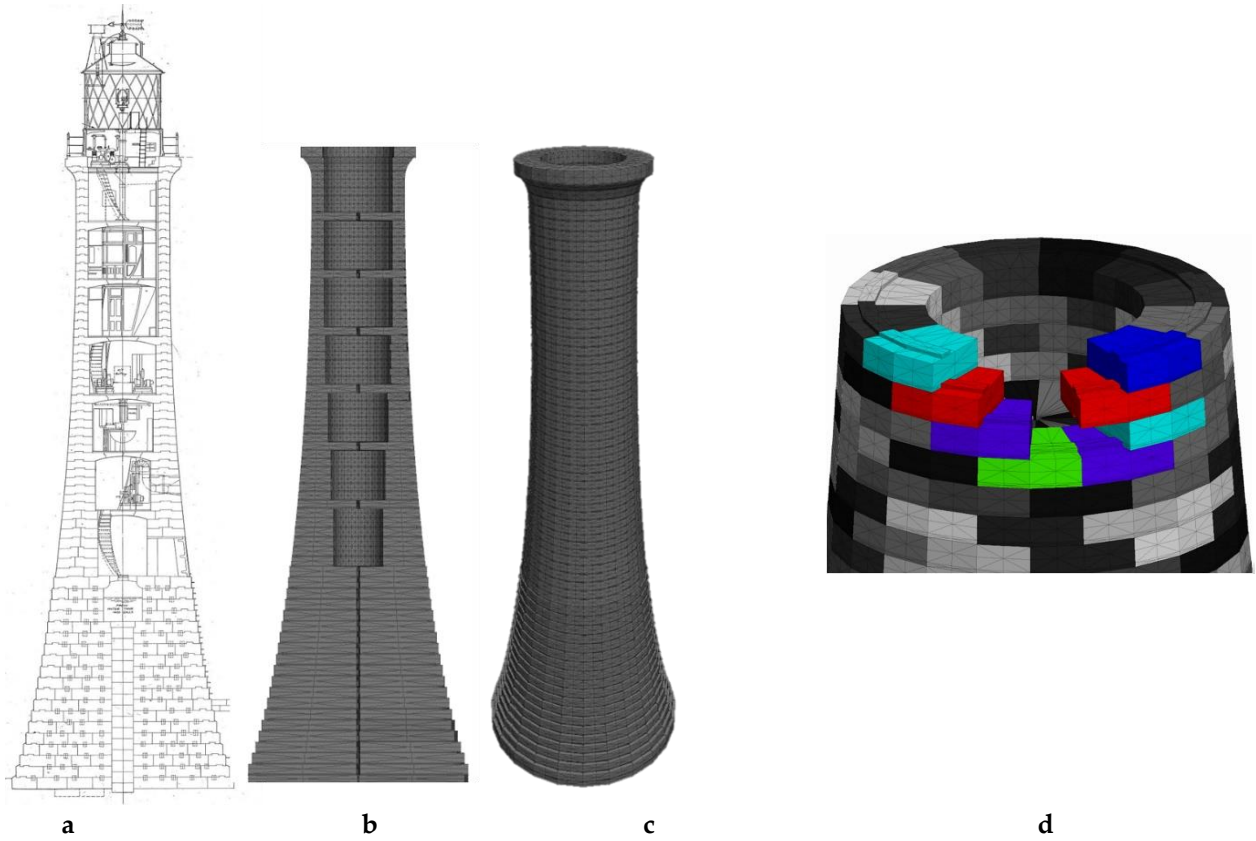

Figure 6. Wolf Rock lighthouse: (**a**) Wolf Rock lighthouse cross-section, 1964 (Trinity house archive [56]); (**b**) 3DEC model section; (**c**) model perspective view; and (**d**) detail of interlocking.

The wave breaks on the Wolf Rock lighthouse between the 23rd and 40th course, at an average height of 13.14 m from the bottom of the structure. The three different pressure distributions are applied as discretised forces along 18 courses of blocks and covering four blocks in each course, resulting in 72 application points (Figure 7).

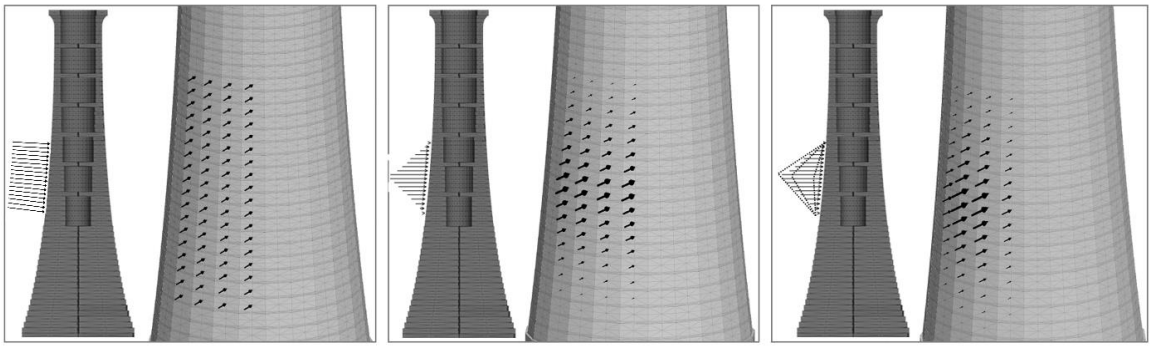

a b c

Figure 7. Pressure profiles in 3DEC: (**a**) distribution #1; (**b**) distribution #2; (**c**) distribution #3.

5. Structural Analysis and Results

Figure 8 presents the structural response, in terms of horizontal and vertical displacement, of a control point on the crown of the tower. The three simulations yield similar responses qualitatively and quantitatively, with the maximum horizontal displacement ranging from 0.219 m to 0.230 m (a difference of up to 5%) and the vertical one between 0.098 m and 0.107 m (a difference of up to 9%). It is interesting to note a relatively high level of damping affecting the structural response before any resonance phenomena occur. The main response outputs are presented in Table 1. Studies on the influence of the wave characteristics have revealed that the structural response of the lighthouse is heavily influenced by parameters such as the force–time history shape, duration and maximum force (Raby et al. (2019), Pappas et al. (2018) [1,2]). For a relative assessment, the current analysis results are compared with the ones manifested by a wave of maximum force equal to 51,149 kN, or just 3.3% higher, with very similar time-history shape and 0.002 s shorter, presented in (Raby et al. (2019) [1]) for a non-stationary case projected at the end of 2067 (refer to [1] for further explanations of the adopted non-stationary Bayesian extreme value analysis to derive design wave climates for the current research study). For that analysis, pressure profile equal to distribution #1 is used, but the impact area is shifted two courses upwards due to the slightly larger wave height and crest (i.e., wave height increased from $H_{0.1\%}$ = 23.25 m to $H_{0.1\%}$ = 25.00 m or by 5.3%). Compared to the results of the distribution #1, the analysis of (Raby et al. (2019) [1]) gives maximum horizontal and vertical displacements 0.276 m and 0.119 m, respectively, or an increase of 20% and 22%, respectively.

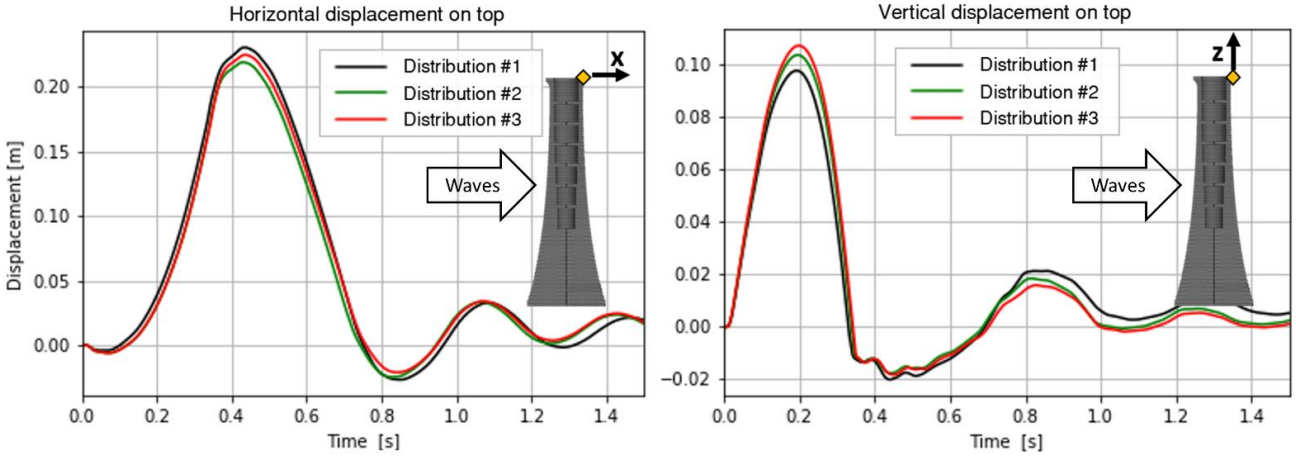

a b

Figure 8. Structural response for the three distributions: (**a**) horizontal displacement; (**b**) vertical displacement.

Table 1. Maximum response values for the three pressure profiles.

	Distribution #1	Distribution #2	Distribution #3
Horizontal displacement on top (m)	0.230	0.219	0.225
Vertical displacement on top (m)	0.098	0.104	0.107
Opening of lower joints on impact side (mm)	5.7	4.8	5.1
Opening of upper joints on opposite side to impact (mm)	22.3	21.6	20.4

Figure 9 shows the amplitude spectra of horizontal and vertical displacements. Two blue vertical lines represent the first and the second natural frequency of Wolf Rock lighthouse: 4.67 Hz and 6.82 Hz, identified during the field modal tests (Raby et al. (2019) [1]). Similar to the displacement results, there is no large difference between the amplitude spectra of the three tested pressure distributions. The peak frequencies (0.5737 Hz for horizontal displacement and 1.434 Hz for vertical displacements) shown here are lower than the first and second natural frequencies identified during the modal tests.

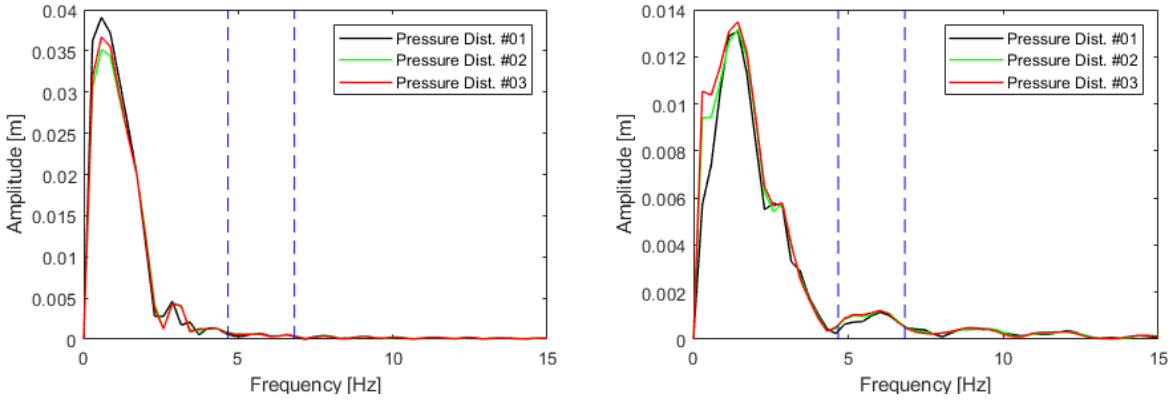

(**a**) Amplitude spectra of horizontal displacements (**b**) Amplitude spectra of vertical displacements

Figure 9. Amplitude spectra of horizontal and vertical displacements.

Indeed, the main aim of the DEM model is to capture the non-linear behaviour of the structure under such massive loading conditions. The combination of intensity, duration and application point of the calculated wave impact force are capable of triggering the lighthouse rocking (non-linear dynamic behaviour), such that the identified natural frequencies are not clearly visible in the response. In other words, the performed modal analysis assumed a fully linear–elastic behaviour of the structure, while the lighthouse under severe wave loading does not behave linearly, thus also the main frequency in the response is different from the identified ones during the field modal test. Furthermore, it must be noted that the direction of impact force (225°) does not align with any of the principal directions, i.e., directions for which no cross effects are present, usually characterised by the maximum and minimum stiffness of the structure.

Another critical response output of the analysis is the maximum joint opening. Sliding failure is prevented by vertical keys, but joint openings larger than the key height may compromise the interlocking effect. When impacted by strong waves, the structure oscillates with the initial opening of lower joints (5 to 6 m below the lowest part of the impact area, i.e., 3.5 to 4.5 m from the lighthouse base) on the impact side and simultaneous opening of upper joints (1 to 1.5 m above the highest part of the impact area, i.e., 16.5 to 17 m from the lighthouse base) on the opposite side. Subsequently, the lower joints close and the

upper joints (around the highest point of the load application area) on the impact side open as the rocking oscillation progresses. This structural behaviour is shown in Figure 10, which presents the opening of the joints on both sides of the lighthouse for the three different distributions.

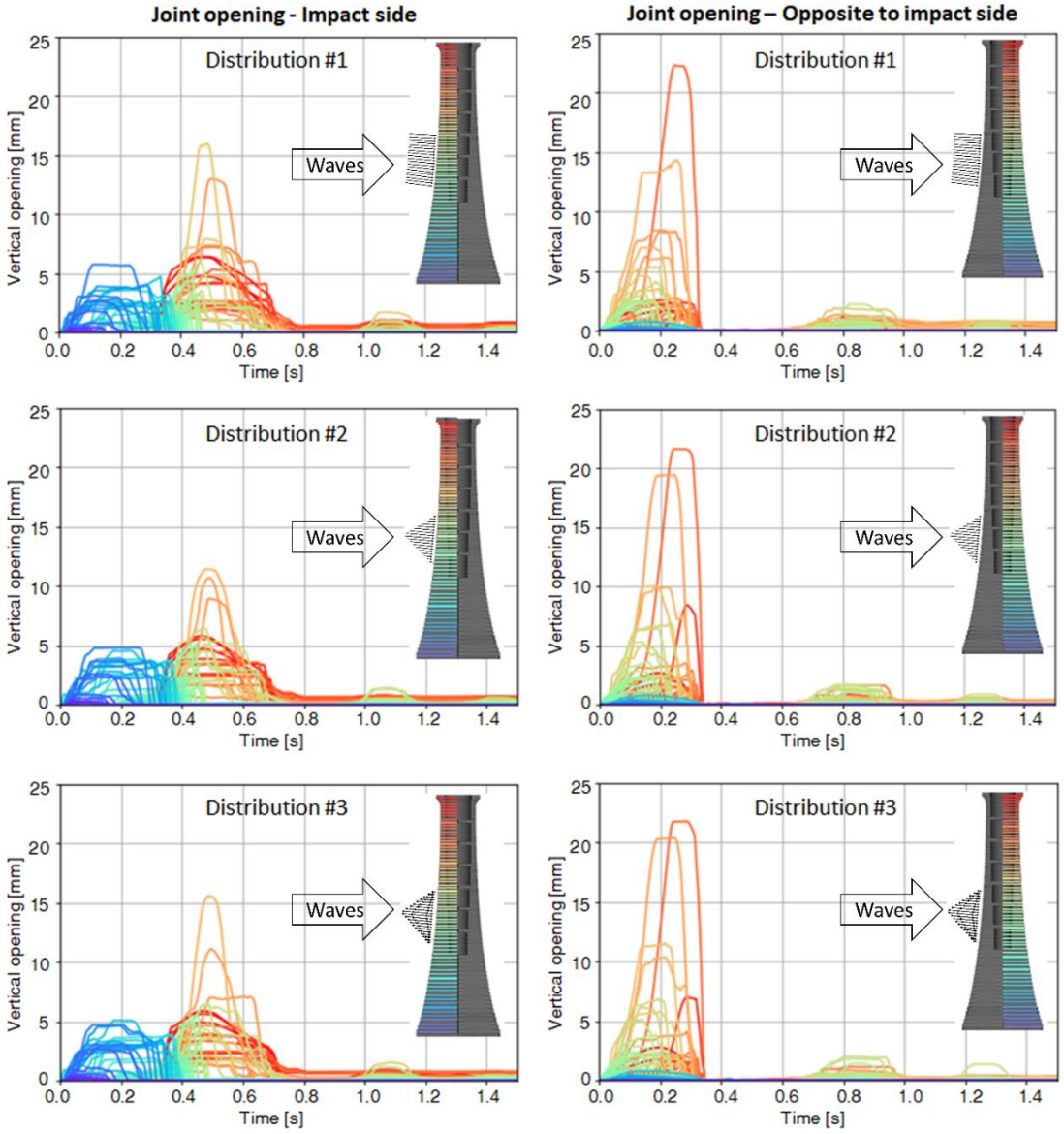

Figure 10. Opening of joints for the three distributions.

For all three analyses, the maximum opening takes place at the joints on the opposite side of the impact and ranges between 20.4 mm and 22.3 mm (Table 1). The maximum opening differs by up to around 9% for the three analyses, which is in the same range as the differences in the maximum vertical displacements. However, apart from the relative quantitative proximity of the results, note the similarity of the time-histories in Figure 10. The same groups of joints are activated at the same periods and the maximum joint opening takes place at exactly the same joint.

6. Conclusions and Outlook

This study evaluated the sensitivity of pressure distribution patterns on the overall structural responses of Wolf Rock lighthouse. Only the initial impulsive portion of the wave loading was considered for the analysis, as this impulsive component is predom-

inately responsible for the structure's dynamic responses. The incident wave direction, the total slamming force (or pressure-integrated force), the total impact area on the surface of the lighthouse and the affected frontal area were kept constant to isolate the effect of the pressure distribution from other contributing variables. The 3D "distinct element method" (DEM) model of the Wolf Rock lighthouse showed relatively larger dynamic responses for pressure distributions #3. Pressure distribution #3 showed the largest vertical displacement and 2nd largest horizontal displacement (only about 2% less horizontal displacement compared to distribution #1) among the different pressure distributions considered in this study. Vertical displacement of pressure distribution #3 was 9% higher than that of pressured distribution #1. Therefore, it can be recommended that future FEM or DEM analysis of vertical cylindrical structures may consider the use of more realistic pressure distributions (similar to pressure distribution #3 considered in this study) rather than simplified distributions (e.g., #1: a uniform pressure distribution). Furthermore, the literature study showed significant temporal variations in the impact area (size and shape), location of the peak pressure within the impact area and pressure distribution patterns. Implementation of the time-varying impact area and pressure distribution is extremely difficult with the existing DEM structural modelling tools; however, it will yield accurate results. A detailed description of the impact pressure distribution (spatial and temporal) can only be achieved through detailed CFD modelling with the real lighthouse and the rock geometries. A CFD study should essentially be supported by either experimental data or field measurements for its calibration and validation since the unique geometry of the lighthouse and the rock created complex wave kinematics. It can be concluded that this paper not only illustrates the sensitivity of the pressure distribution pattern on the dynamic response of the Work Rock lighthouse but also highlights its importance and the lack of comprehensive understanding about its quantitative description.

Author Contributions: A.A., A.R., J.M.W.B., and D.D. conceived and designed this numerical modelling study; A.P. performed the numerical simulations; A.P. and D.D. analyzed the data; A.A. and D.T.D. contributed with analysis tools and further data analysis; D.T.D. and A.P. wrote the paper and A.R. performed a thorough review. All authors have read and agreed to the published version of the manuscript.

Funding: This research has been undertaken as part of the STORMLAMP project, funded by the EPSRC (EP/N022947/1, EP/N022955/1 and EP/N023285/1) and the UK and Irish General Lighthouse Authorities (GLAs).

Institutional Review Board Statement: Not applicable for studies not involving humans or animals.

Informed Consent Statement: Not applicable for studies not involving humans.

Data Availability Statement: The data presented in this study are available on request from the corresponding author.

Conflicts of Interest: The authors declare no conflict of interest.

References

1. Raby, A.C.; Antonini, A.; Pappas, A.; Dassanayake, D.T.; Brownjohn, J.M.W.; D'Ayala, D. Wolf Rock lighthouse: Past developments and future survivability under wave loading. *Philos. Trans. R. Soc. A Math. Phys. Eng. Sci.* **2019**, *377*. [CrossRef]
2. Pappas, A.; D'Ayala, D.; Antonini, A.; Raby, A. Rock mounted iconic lighthouses under extreme wave impacts: Limit Analysis and Discrete Element Method. In Proceedings of the 9th International Conference on Computational Methods—ICCM2018, Rome, Italic, 18 June 2018; p. 13.
3. Wienke, J.; Oumeraci, H. Breaking wave impact force on a vertical and inclined slender pile—theoretical and large-scale model investigations. *Coast. Eng.* **2005**, *52*, 435–462. [CrossRef]
4. Boyle, M. *Wolf Rock (Lighthouses of England & Wales S.)*; B & T Publications: Highfield, UK, 1998; ISBN 978-1901043075.
5. Nicholson, C. *Rock Lighthouses of Britain*; Whittles Publishing: Dunbeath, UK, 2015; ISBN 978-184995-214-9.
6. Douglass, J.N. The wolf rock lighthouse. *Minutes Proc. Inst. Civ. Eng.* **1870**, *30*, 1–28. [CrossRef]
7. Douglass, J.N. On the Wolf Rock Lighthouse. *Minutes Proc. Inst. Civ. Eng.* **1871**, *49*, 214–227.
8. Antonini, A.; Raby, A.; Brownjohn, J.M.W.; Pappas, A.; D'Ayala, D. Survivability assessment of Fastnet lighthouse. *Coast. Eng.* **2019**, *150*, 18–38. [CrossRef]

9. Trinh, Q.; Raby, A.; Banfi, D.; Corrado, M.; Chiaia, B.; Rafiq, Y.; Cali, F. Modelling the Eddystone Lighthouse response to wave loading. *Eng. Struct.* **2016**, *125*, 566–578. [CrossRef]
10. Banfi, D. A Field and Laboratory Study on the Dynamic Response of the Eddystone Lighthouse to Wave Loading. Ph.D. Thesis, University of Plymouth, Plymouth, UK, 2018.
11. Tanimoto, K.; Takahashi, S.; Kaneko, T.; Shiota, K. Impulsive breaking wave forces on an inclined pile exerted by random waves. In *Proceedings of the Twentieth Int. Conf. on Coastal Engineering*; Edge, B.L., Ed.; American Society of Civil Engineers: Taipei, Taiwan, 1986; Volume III, pp. 2288–2302.
12. Veić, D.; Sulisz, W. Impact Pressure Distribution on a Monopile Structure Excited by Irregular Breaking Wave. *Polish Marit. Res.* **2018**, *25*, 29–35. [CrossRef]
13. Trinity House Eddystone Lighthouse. Available online: https://www.trinityhouse.co.uk/lighthouses-and-lightvessels/eddystone-lighthouse (accessed on 3 January 2021).
14. Goda, Y. *Random Seas and Design of Maritime Structures*, 3rd ed.; World Scientific Publishing Co. Pte. Ltd.: Singapore, 2010; Volume 33.
15. Battjes, J.A.; Groenendijk, H.W. Wave height distributions on shallow foreshores. *Coast. Eng.* **2000**, *40*, 161–182. [CrossRef]
16. Morison, J.R.; Johnson, J.W.; Schaaf, S.A. The force exerted by surface waves on piles. *J. Pet. Technol.* **1950**, *2*, 149–154. [CrossRef]
17. Morison, J.R.; Johnson, J.W.; O'Brien, M.P. Experimental Studies of Forces on Piles. In *Proceedings of the 4th Conference on Coastal Engineering*; Johnson, J.W., Ed.; Council On Wave Research, The Engineering Foundation: Chicago, IL, USA, 1953; Volume 1, p. 25.
18. DNV. *Design of Offshore Wind Turbine Structures*; Det Norske Veritas (DNV): Oslo, Norway, 2014.
19. Corvaro, S.; Crivellini, A.; Marini, F.; Cimarelli, A.; Capitanelli, L.; Mancinelli, A. Experimental and numerical analysis of the hydrodynamics around a vertical cylinder in waves. *J. Mar. Sci. Eng.* **2019**, *7*, 453. [CrossRef]
20. Goda, Y.; Haranaka, S.; Kitahata, M. *Study on Impulsive Breaking Wave Forces on Piles*; Port and Harbour Research Institute Ministry of Transport: Yokosuka, Japan, 1966; Volume 6.
21. Chaplin, J.R.; Subbiah, K.; Irani, M. Local Forces On A Vertical Cylinder In Regular And Irregular Waves. In Proceedings of the Second International Offshore and Polar Engineering Conference, San Francisco, CA, USA, 14–19 June 1992; p. 7.
22. Wienke, J. *Druckschlagbelastung auf Schlanke Zylindrische Bauwerke Durch Brechende Wellen theoretische und großmaßstäbliche Laboruntersuchungen*; Technischen Universität Braunschweig: Braunschweig, Germany, 2001.
23. Ghadirian, A.; Bredmose, H. Pressure impulse theory for a slamming wave on a vertical circular cylinder. *J. Fluid Mech.* **2019**, *867*, R1. [CrossRef]
24. Wiegel, R.L. Forces induced by breakers on piles. In Proceedings of the 18th International Conference on Coastal Engineering, Cape Town, South Africa, 14–19 November 1982; pp. 1699–1715.
25. Watanabe, A.; Horikawa, K. Breaking wave forces on a large diameter cell. In Proceedings of the 14th International Conference on Coastal Engineering, Copenhagen, Denmark, 24–28 June 1974; pp. 1741–1760.
26. Sawaragi, T.; Nochino, M. Impact Forces of Nearly Breaking Waves on a Vertical Circular Cylinder. *Coast. Eng. Jpn.* **1984**, *27*, 249–263. [CrossRef]
27. Apelt, C.J.; Piorewicz, J. Impact Force as a Part of the Total Breaking Wave Force on a Vertical Cylinder. In Proceedings of the 10th Australasian Conference on Coastal and Ocean Engineering, Auckland, New Zealand, 2–6 December 1991; Bell, R.G., Hume, T.M., Terry, R., Eds.; Water Quality Centre publication: Hamilton, New Zealand, 1991; pp. 404–409.
28. Alagan Chella, M.; Bihs, H.; Myrhaug, D. Wave impact pressure and kinematics due to breaking wave impingement on a monopile. *J. Fluids Struct.* **2019**, *86*, 94–123. [CrossRef]
29. Von Karman, T. *The Impact on Seaplane Float during Landing*; National Technical Information Service, U.S.; Department of Commerce: Washington, DC, USA, 1929.
30. Wagner, H. Über Stoß- und Gleitvorgänge an der Oberfläche von Flüssigkeiten. *ZAMM -Zeitschrift Angew. Math. Mech.* **1932**, *12*, 193–215. [CrossRef]
31. Irschik, K.; Sparboom, U.; Oumeraci, H. Breaking Wave Characteristics for the Loading of a Slender Pile. In Proceedings of the 28th International Conference on Coastal Engineering, Cardiff, Wales, 7–12 July 2002; pp. 1341–1352.
32. Kyte, A.; Tørum, A. Wave forces on vertical cylinders upon shoals. *Coast. Eng.* **1996**, *27*, 263–286. [CrossRef]
33. Goda, Y.; Ikeda, T.; Sasada, T.; Kishida, Y. *Study on Design Wave Forces on Circular Cylinders Erected upon Reefs*; Nahase: Yokisuka, Japan, 1972.
34. Zhou, D.; Chan, E.S.; Melville, W.K. Wave impact pressures on vertical cylinders. *Appl. Ocean Res.* **1991**, *13*, 220–234. [CrossRef]
35. Tuan, T.Q.; Cuong, D.Q. Distribution of wave heights on steep submerged reefs. *Ocean Eng.* **2019**, *189*, 106409. [CrossRef]
36. Palmer, M.; Howard, T.; Tinker, J.; Lowe, J.; Bricheno, L.; Calvert, D.; Edwards, T.; Gregory, J.; Harris, G.; Krijnen, J.; et al. *UKCP18 Marine Projection Report [UK Climate Projections (UKCP)], Met Office, UK*; Environment Agency: Exeter, UK, 2018.
37. Hansen, J.B. Periodic waves in the surf zone: Analysis of experimental data. *Coast. Eng.* **1990**, *14*, 19–41. [CrossRef]
38. Ganderton, P. *Wolf Rock Drone Survey Results, School of Biological and Marine Sciences*; Faculty of Science and Engineering, University of Plymouth: Plymoouth, UK, 2019.
39. Trinity House. *Single Beam Echo Sounder Survey of Wolf Rock Lighthouse (Galatea/P28, Surveyed date: 04.07.19), The Corporation of Trinity House*; The Corporation of Trinity House: London, UK, 2019.
40. Grimshaw, R. The solitary wave in water of variable depth. Part 2. *J. Fluid Mech.* **1971**, *46*, 611–622. [CrossRef]
41. Douglass, W.T.; Webb, S.; Owen, G.W.; Redman, J.B.; Beazeley, M.; Harcourt, L.F.V.; Williams, P.; Inglis, J.C.; Rawlinson, S.R.; Brunton, R.H.; et al. Discussion on the new Eddystone Lighthouse. *Minutes Proc. Inst. Civ. Eng.* **1884**, *75*, 37–56. [CrossRef]

42. Pappas, A.; D'Ayala, D.; Antonini, A.; Raby, A. Finite Element Modelling and Limit Analysis of Fastnet Lighthouse Under Impulsive Ocean Waves. In Proceedings of the International Conference on Structural Analysis of Historical Constructions, Cusco, Peru, 11–13 September 2019; Aguilar, R., Torrealva, D., Moreira, S., Pando, M.A., Eds.; Springer: Singapore, 2019; Volume 18, pp. 881–890.
43. Pappas, A.; D'Ayala, D.; Dassanayake, D.T.; Antonini, A.; Raby, A. Rocking of offshore lighthouses under extreme wave impacts: Limit Analysis, Analytic formulations and Distinct Element Method. *Eng. Struct.* **2020**, *228*, 11153. [CrossRef]
44. Housner, G. The behavior of inverted pendulum structures during earthquakes. *Bull. Seismol. Soc. Am.* **1963**, *53*, 403–417.
45. Ishiyama, Y. Motions of rigid bodies and criteria for overturning by earthquake excitations. *Bull. New Zeal. Soc. Earthq. Eng.* **1984**, *17*, 24–37. [CrossRef]
46. Yim, C.; Chopra, A.; Penzien, J. Rocking response of rigid blocks to earthquakes. *Earthq. Eng. Struct. Dyn.* **1980**, *8*, 565–587. [CrossRef]
47. Spanos, P.; Asce, M.; Koh, A.; Asce, A.M. Rocking of rigid blocks due to harmonic shaking. *J. Eng. Mech.* **1984**, *110*, 1627–1642. [CrossRef]
48. Lemos, J.V. Discrete Element Modeling of Masonry Structures. *Int. J. Archit. Herit.* **2007**, *1*, 190–213. [CrossRef]
49. Giandomenico, R. Explicit Finite Difference Methods. *SSRN Electron. J.* **2017**, 132–150. [CrossRef]
50. Cundall, P. A computer model for simulating progressive large-scale movements in blocky rock system. In Proceedings of the Symposium of the International Society of Rock Mechanics, Nancy, France, 4–6 October 1971; pp. 132–150.
51. Lajtai, E.Z.; Gadi, A.M. Friction on a granite to granite interface. *Rock Mech. Rock Eng.* **1989**, *22*, 25–49. [CrossRef]
52. Itasca Inc. *3DEC 5.0: 3-Dimensional Distinct Element Code, Theory and Background*; Itasca Inc.: Minneapolis, MN, USA, 2013.
53. Pappas, A.; D'Ayala, D.; Antonini, A.; Brownjohn, J.; Raby, A. Numerical modelling of Fastnet lighthouse based on experimental dynamic identification. In Proceedings of the International Conference on Advances in Construction Materials and Systems ICACMS-2017, Chennai, India, 3–8 September 2017; pp. 1–10.
54. Brownjohn, J.M.W.; Raby, A.; Au, S.K.; Zhu, Z.; Wang, X.; Antonini, A.; Pappas, A.; D'Ayala, D. Bayesian operational modal analysis of offshore rock lighthouses: Close modes, alignment, symmetry and uncertainty. *Mech. Syst. Signal Process.* **2019**, *133*, 106306. [CrossRef]
55. Brownjohn, J.M.W.; Raby, A.; Bassitt, J.; Antonini, A.; Hudson, E.; Dobson, P. Experimental modal analysis of British rock lighthouses. *Mar. Struct.* **2018**, *62*, 1–22. [CrossRef]
56. Trinity House Archives Wolf Rock Lighthouse Section Elevation and FLoor Plans, Re-drwn supersedes P.170 tracing by Happer and Tunstall in July 1866, DRG. No. 85/96, Drawn by M.G.M. 1964, 1. Available online: https://www.archives.gov/files/publications/lists/special-list-57.pdf (accessed on 21 December 2020).